Available online at www.sciencedirect.com
SCIENCE DIRECT®
Polymer 44 (2003) 5429–5437
polymer
www.elsevier.com/locate/polymer

Crystallization behaviour of biodegradable poly(ethylene succinate) from the amorphous state

Zhaobin Qiu[a,b,*], Takayuki Ikehara[a,c], Toshio Nishi[a,b,*]

[a]*Department of Applied Physics, School of Engineering, The University of Tokyo, 7-3-1, Hongo, Bunkyo-ku, Tokyo 113-8656, Japan*
[b]*Department of Organic and Polymeric Materials, Graduate School of Science and Engineering, Tokyo Institute of Technology, 2-12-1 Ohokayama, Meguro-ku, Tokyo 152-8552, Japan*
[c]*Department of Applied Chemistry, Faculty of Engineering, Kanagawa University, 3-27-1, Rokkakubashi, Kanagawa-ku, Yokohama 221-8686, Japan*

Received 26 March 2003; received in revised form 31 May 2003; accepted 27 June 2003

Abstract

Nonisothermal and isothermal crystallization kinetics of biodegradable poly(ethylene succinate) (PES) from the amorphous state were studied by differential scanning calorimetry (DSC). For the nonisothermal crystallization, there were two crystallization exotherms upon heating from the amorphous state. One major crystallization exotherm located at low temperature corresponded to the real cold crystallization of PES, while the other minor one located at high temperature may correspond to the melt-recrystallization of the unstable crystals formed during the nonisothermal crystallization earlier. Several methods, such as Avrami equation, Tobin equation and Ozawa equation, were applied to describe the nonisothermal crystallization process of PES. Meanwhile, Avrami equation was also employed to study the isothermal crystallization of PES from the amorphous state. Similar to the nonisothermal crystallization the minor crystallization exotherm was also found in the DSC trace upon heating to the melt after the isothermal cold crystallization finished completely, and was attributed to the melt-recrystallization of the unstable crystals formed during the isothermal cold crystallization. Temperature modulated differential scanning calorimetry (TMDSC) was used in this work to investigate the origin of the minor crystallization exotherm located at high temperature, and the TMDSC experiments gave a direct evidence that the origin of the minor crystallization exotherm was from the melt-recrystallization of the originally existed unstable crystals formed through previous crystallization.

Keywords: Poly(ethylene succinate); Crystallization; Temperature modulated differential scanning calorimetry

1. Introduction

Biodegradable polymers have attracted considerable attention due to their potential applications in the fields related to human life such as environmental protection and the maintenance of physical health in the last two decades. Among them poly(hydroxybutyrate) (PHB) is probably the most extensively studied biodegradable thermoplastic polymer. Ha et al. recently reviewed the miscibility, properties and biodegradability of blends containing either PHB or poly(3-hydroxybutyrate-*co*-hydroxyvalerate) [1].

Poly(ethylene succinate) (PES) is one of the biodegradable synthetic polyesters; however, it has not been paid enough attention till now compared with the study of PHB. The chemical structure of PES is $(-OCH_2CH_2O_2CCH_2CH_2CO-)n$. The crystal structure of PES was first studied by Fuller et al. using X-ray diffraction in 1937, and a monoclinic unit cell with dimensions $a = 0.905$ nm, $b = 1.109$ nm, c(fiber axis) $= 0.832$ nm, and $\beta = 102.8°$ was proposed [2]. The crystal and molecular structures of PES were determined by Ueda et al. again using X-ray diffraction in 1971[3], who made a slight modification of the crystallographic data. PES crystallized as a $Pbnb$-D_{2h}^{10} space group with unit cell parameters $a = 0.760$ nm, $b = 1.075$ nm, and c(fiber axis) $= 0.833$ nm, and four molecular chains pass through the unit cell [3]. Recently, Iwata et al. confirmed the crystal structure of PES proposed by Ueda et al. through the study on solution-grown crystals using electron microscopy [4]. Ichikawa et al. once reported the crystal modification

* Corresponding authors. Address: Department of Organic and Polymeric Materials, Graduate School of Science and Engineering, Tokyo Institute of Technology, 2-12-1 Ohokayama, Meguro-ku, Tokyo 152-8552, Japan. Tel./fax: +81-357-343-507.
E-mail addresses: tnishi@polymer.titech.ac.jp (T. Nishi), zbqiu99@yahoo.com (Z. Qiu).

0032-3861/03/$ - see front matter © 2003 Elsevier Ltd. All rights reserved.
doi:10.1016/S0032-3861(03)00577-9

β-form of strained PES fiber and the fiber repeat period was 0.95 nm [5]. Al-Raheil et al. studied the morphology of melt-crystallized PES by optical microscopy and scanning electron microscopy and the melting behaviour of PES by differential scanning calorimetry (DSC) [6]. They found that at low crystallization temperature imperfect crystals were formed which could melt and recrystallize during the DSC scan so that triple melting peaks were observed. However, at high crystallization temperature perfect crystals (dominant and subsidiary lamellae in the spherulitic structure) were formed so that two melting peaks were observed which was explained by the existence of two kinds of crystal perfection. Gan et al. studied the morphology and crystallization kinetics of PES using OM and atomic force microscopy, who found that there was a crystallization regime transition between regime III and regime II at ca. 71 °C and the ratio of the nucleation constant K_g^{III} to K_g^{II} was influenced strongly by the values of the activation energy U^* used for transporting the polymer chain segments to the crystallization site [7]. The crystallization and morphology of PES in binary miscible blends of two crystalline polymers were also reported recently, such as in PES/PHB and PES/poly(ethylene oxide) (PEO) blends [8,9]. In our previous work, we reported that PES and PEO could form interpenetrated spherulites at 50 °C for PES/PEO 20/80 blend through the OM study [10].

It is well known that the physical properties and biodegradability of biodegradable polymers are influenced strongly by the crystallinity. Meanwhile, the crystalline structure and morphology of semicrystalline polymers are also influenced greatly by the thermal history. Therefore, the crystallization kinetics study should be paid enough attention, since it not only affects the crystalline structure and morphology of semicrystalline polymers but also affects the final physical properties and biodegradability for the biodegradable polymers. However, till now only Gan et al. investigated the crystallization kinetics of PES from the melt by studying the spherulitic growth rate with OM [7]. To our knowledge, the overall crystallization kinetics of PES has not been reported so far in the literature. In the present paper, we reported our studies on the overall crystallization kinetics study of PES from the amorphous state by DSC, and the crystallization from the melt is still underway and will be reported in a separate manuscript.

2. Experimental

PES used in this study was purchased from the Aldrich Chemical Company, catalogue no. 18203-6. The samples were received in the form of chunks.

Nonisothermal and isothermal crystallization studies were carried out using a Perkin Elmer differential scanning calorimeter (DSC-7). Indium and zinc standards were used for temperature calibration. Samples weight varied about 4–6 mg, and all operations were performed under nitrogen. For nonisothermal crystallization studies, the samples were first quenched to −40 °C at 200 °C/min after melted at 150 °C for 3 min to reach the amorphous state, and then heated to 150 °C at various heating rates Φ, ranging from 2.5 to 100 °C/min. The exothermal curves of heat flow as a function of temperature were recorded and analyzed. For isothermal crystallization studies, the samples were first quenched to −40 °C at 200 °C/min after melted at 150 °C for 3 min to reach the amorphous state, and then heated to the predetermined crystallization temperatures T_c (22–30 °C) at 80 °C/min. The exothermal curves of heat flow as a function of time were recorded and investigated. The samples were heated to 150 °C at 20 °C/min after they completed the isothermal crystallization.

A TA 2910 temperature modulated DSC was used for TMDSC analysis. All scans were run under a nitrogen gas purge to minimize thermo-oxidative degradation. For the TMDSC measurements, the heating was operated at 2 °C/min with the oscillation amplitude of 0.5 °C, and the oscillation period of 40 s throughout the investigation.

3. Results and discussion

3.1. Nonisothermal crystallization kinetics study

Crystalline polymers are able to crystallize between the glass transition temperature (T_g) and the melting point temperature (T_m). According to the difference in the initial state, the crystallization process can be classified into two categories. One is called melt crystallization, which means the initial state is the molten state and the polymer samples should stay at a temperature higher than its T_m first. The other is called cold crystallization, which means the initial state is the amorphous state and the polymer samples should stay in a temperature lower than its T_g first. In general, crystalline polymers are able to crystallize either from the melt or from the amorphous state. In this paper, the crystallization of PES from the amorphous state was studied. It is essential to study the kinetics of nonisothermal crystallization since most polymer processing operations are carried out under nonisothermal conditions. Therefore, the nonisothermal crystallization kinetics study of PES from the amorphous state was studied by DSC first.

As described in the Section 2, the samples were first quenched from the melt to −40 °C to reach the amorphous state and then heated to 150 °C at various heating rates to study the crystallization kinetics and melting behaviour of PES from the amorphous state. Fig. 1 showed the DSC traces of PES heated from the amorphous state at various heating rates. One peculiar phenomenon was observed that two crystallization exotherms appeared when PES crystallized from the amorphous state at the heating rate ≤40 °C/min. One major exothermal peak T_{c1} located at the low temperature range and shifted apparently to the high temperature range with the heating rate. And the other

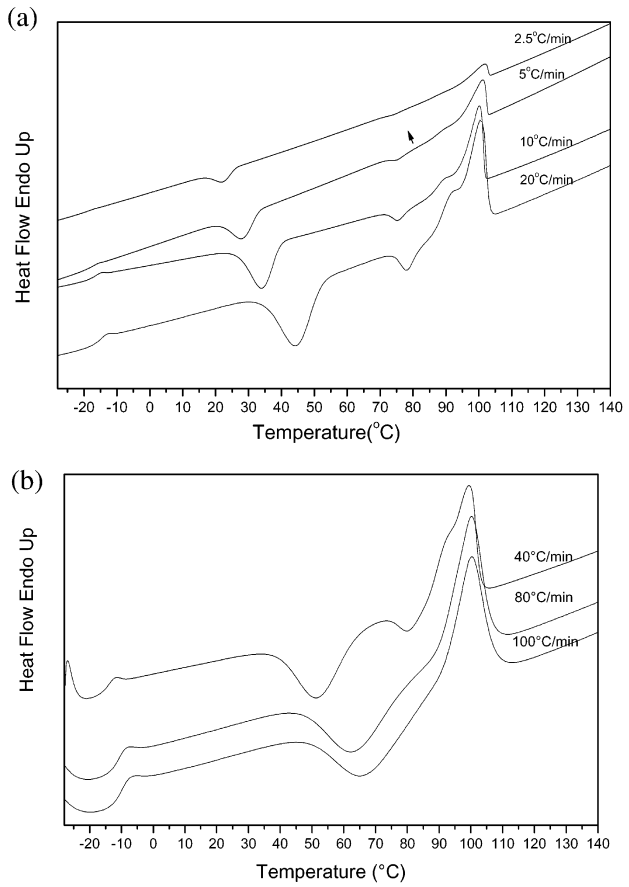

Fig. 1. DSC traces of PES heated from the amorphous state at various heating rates, (a) low heating rates and (b) high heating rates.

minor exothermal peak T_{c2} located at high temperature around 75 °C, and was almost unchanged at the heating rate $\leq$10 °C/min. However, it should be noted that with increasing the heating rate T_{c1} appeared and shifted to high temperature range, while T_{c2} diminished gradually and disappeared, especially at 80 and 100 °C/min. Therefore it was apparent that T_{c1} was the real cold crystallization exotherm for PES upon heating from the glassy state above T_g. As to T_{c2}, it may correspond to the melt-recrystallization of the unstable crystals formed during the nonisothermal crystallization earlier and would be discussed in the following section in detail.

In this paper, only the T_{c1} obtained by the low heating rates $\leq$20 °C/min were used to study the kinetics of nonisothermal crystallization of PES for the sake of the accuracy of the data collected from DSC. Integration of the exothermic peak during the nonisothermal scan shown in Fig. 1(a) gave the relative crystallinity as a function of temperature (Fig. 2). The plot of relative crystallinity versus crystallization temperature shifted to the high temperature range with the heating rate.

During the nonisothermal crystallization from the amorphous at a constant heating rate, the relationship between the crystallization time t and the crystallization

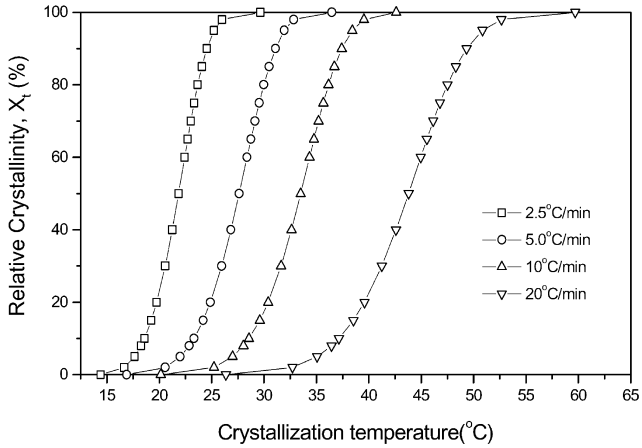

Fig. 2. Plots of relative crystallinity versus crystallization temperature for PES during nonisothermal crystallization from the amorphous state.

temperature T could be described as

$$t = \frac{T - T_0}{\Phi} \quad (1)$$

where Φ was the heating rate, and T_0 was the onset temperature of crystallization. Fig. 3 showed the relative crystallinity as a function of crystallization time by using Eq. (1) for PES. It could be seen from Fig. 3 that the lower the heating rate, the longer the crystallization time.

Three methods, namely Avrami [11], Tobin [12] and Ozawa equations [13], were employed to investigate the kinetics of nonisothermal crystallization of PES in this work.

The well-known Avrami equation is often used to analyze the isothermal crystallization kinetics; it assumes that the relative degree of crystallinity development with crystallization time t is

$$X_t = 1 - \exp(-k_a t^{n_a}) \quad (2)$$

where n_a is the Avrami exponent depending on the nature of nucleation and growth geometry of the crystals, and k_a is a composite rate constant involving both nucleation and growth rate parameters [11].

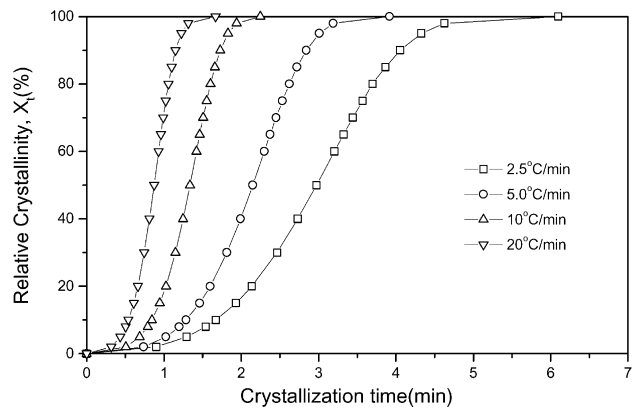

Fig. 3. Plots of relative crystallinity versus crystallization time for PES during nonisothermal crystallization from the amorphous state.

Although, the Avrami equation is often used to study the isothermal crystallization behaviour of polymers, it has also been applied directly to describe the nonisothermal crystallization of polymers [14,15]. Using Eq. (2) in its double-logarithmic form, and plotting $\log(-\ln(1-X_t))$ against $\log t$ for each heating rate as shown in Fig. 4, a series of straight lines were obtained, from which the values of the two adjustable parameters, n_a and k_a, were obtained and listed in Table 1. Here, it must be emphasized that in the nonisothermal crystallization the values of n_a and k_a do not have the same physical significance as in the isothermal crystallization due to the fact that under nonisothermal condition the temperature changes constantly. This must affect the rates of both nuclei formation and spherulite growth since they are both temperature dependent. Therefore, in this case, n_a and k_a are only two adjustable parameters to be fitted to the data obtained from the nonisothermal crystallization process. Although, the physical meaning of n_a and k_a cannot be related in a simple way to the isothermal case, the direct application of the Avrami equation does provide further insight into the kinetics of nonisothermal crystallization [14]. In the case of the nonisothermal crystallization of PES from the amorphous state, it can be concluded from Fig. 4 and Table 1 that the crystallization mechanism of PES does not change with the heating rates since a series of almost parallel straight lines were obtained and the slopes of the almost parallel straight lines, namely the Avrami exponents n_a, varied slightly around 4. Although, the values of n_a cannot be related to the crystallization mechanism as in the case of isothermal crystallization, we do believe that the crystallization mechanism of PES remains almost the same despite the change of the heating rates. Actually, strictly speaking, even in the case of isothermal crystallization, an unequivocal relationship between the Avrami exponent n_a and the crystallization mechanism should not be established from the thermal measurements alone without the morphology observation study by optical microscopy and so on.

Table 1
Nonisothermal crystallization kinetics of PES from the amorphous state based on the Avrami equation and the Tobin equation

Φ (°C/min)	n_a	k_a ($\min^{-n_a}$)	n_t	k_t ($\min^{-n_t}$)
2.5	3.51	1.60×10^{-2}	4.47	8.96×10^{-3}
5.0	3.91	3.63×10^{-2}	4.99	2.55×10^{-2}
10.0	4.33	0.20	5.54	0.23
20.0	4.13	1.26	5.30	2.38

n_a : Avrami exponent, k_a : Avrami crystallization rate constant; n_t : Tobin exponent, k_t : Tobin crystallization rate constant.

Meanwhile, it can be concluded from Fig. 4 and Table 1 that the crystallization rate increases with the heating rates. The higher the heating rates, the shorter the crystallization time. Finally, it should be noted again that when the Avrami equation is employed directly to describe the nonisothermal crystallization, n_a and k_a are only two adjustable parameters to be fitted to the data obtained from the nonisothermal crystallization process.

Tobin proposed a theory of phase transformation kinetics with growth site impingement to describe the nonisothermal crystallization process of polymers [12]. According to this approach, the equation of phase transition is

$$X_t = \frac{k_t t^{n_t}}{1 + k_t t^{n_t}} \tag{3}$$

where X_t is the relative crystallinity as a function of time, k_t is the Tobin crystallization rate constant, and n_t is the Tobin exponent. Based on this proposition, the Tobin exponent n_t does not need to be integral, since it is controlled directly by different types of nucleation and growth mechanism. Eq. (3) could be rewritten as follows to calculate the Tobin crystallization kinetics parameters

$$\log(X_t/(1-X_t)) = \log k_t + n_t \log t \tag{4}$$

The Tobin exponent n_t and k_t could be obtained from the plots of $\log(X_t/(1-X_t))$ versus $\log t$ shown in Fig. 5 and listed in Table 1, too.

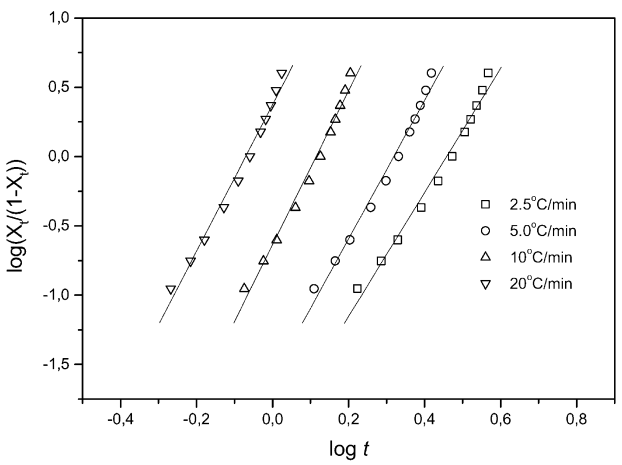

Fig. 4. Avrami plots of PES during nonisothermal crystallization from the amorphous state.

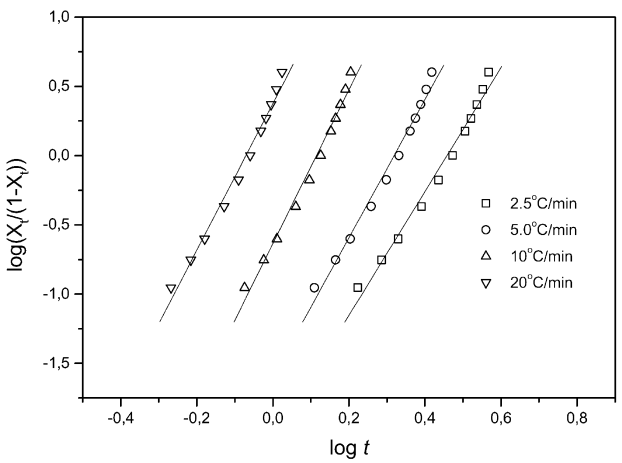

Fig. 5. Tobin plots of PES during nonisothermal crystallization from the amorphous state.

It was interesting to compare the results obtained from the Avrami method and the Tobin approach. From Table 1, it was clear that at the same heating rate the value of Avrami exponent n_a was always smaller than that of the Tobin exponent n_t. By taking the average of the difference between the two values, it could be concluded that $n_t \approx n_a + 1.1$. Similar results were also found for syndiotactic polypropylene (s-PP) [16]. The relative crystallinity X_t was reconstructed as a function of crystallization time for each heating rate using the mathematical Eqs. (2) and (3) in order to test the efficiency of both methods in describing the non-isothermal crystallization process of PES. Based on the kinetics parameters listed in Table 1, the reconstructed X_t was shown in Fig. 6, in which the Avrami prediction was shown as solid lines, whereas the Tobin prediction was shown in dashed lines. It was clear that both methods could provide a good fit to the experimental data for the majority of X_t. However, in the higher X_t range ($X_t \geq 75\%$), the Tobin method always gave the low value compared with the experimental data. The reasons might be that the model as shown in Eq. (3) was the simplified form of a rather more complicated model described in the original publications, or perhaps due to the overemphasis of the impingement effect. Similar results were also found for s-PP [16].Compared with the Tobin method, the Avrami model could fit almost the whole range of X_t very well.

Ozawa extended the Avrami equation for isothermal crystallization to the nonisothermal case by assuming that the sample was cooled (or heated) with a constant rate from the molten state (or the amorphous state) [13]. In the Ozawa method, the time variable in the Avrami equation was replaced by a cooling (or heating) rate and the relative crystallinity was derived as a function of constant cooling (or heating) rate Φ as

$$X_t = 1 - \exp\left(\frac{-K(T)}{\Phi^{n_o}}\right) \tag{5}$$

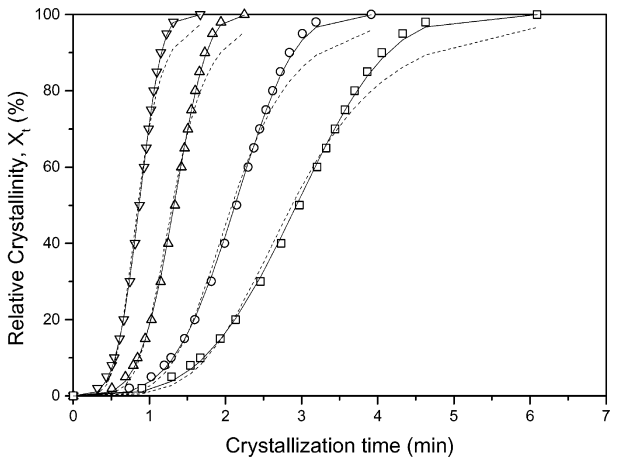

Fig. 6. Model prediction based on the Avrami and the Tobin equations are shown as solid and dashed lines, respectively, to fit the experimental relative crystallinity as a function of crystallization time for various heating rates (°C/min): (□) 2.5; (○) 5; (Δ) 10; (▽) 20.

where $K(T)$ is the cooling (or heating) function at crystallization temperature T and n_o is the Ozawa exponent which depends on the type of nucleation and growth mechanism. Double logarithms of Eq. (5) and rearrangement resulted in the following form:

$$\log(-\ln(1 - X_t)) = \log K(T) - n_o \log \Phi \tag{6}$$

Fig. 7 showed the Ozawa plots of $\log(-ln(1 - X_t))$ versus $\log \Phi$ for PES, from which the Ozawa exponent n_o and the heating function $K(T)$ were obtained and listed in Table 2. It could be seen that the value of the Ozawa exponent n_o was between 3.0 and 4.0, which suggested that the crystallization might correspond to the three dimensional spherulite with thermal nucleation [17].

The activation energy of crystallization could be derived from the Kissinger method in the following form:

$$\frac{d\left(\ln\left(\frac{\Phi}{T_p^2}\right)\right)}{d\left(\frac{1}{T_p}\right)} = -\frac{\Delta E}{R} \tag{7}$$

where ΔE is the activation energy, T_p is the crystallization peak temperature with the maximum crystallization rate of DSC curves, and R is the universal gas constant [18]. The slopes of the plots of $\ln(\Phi/T_p^2)$ versus $1/T_p$ gave the value of $-\Delta E/R$ (Fig. 8). Thus, the activation energy ΔE of nonisothermal crystallization was estimated to be 34.03 kJ/mol.

3.2. Isothermal crystallization kinetic study

The isothermal crystallization of PES from the amorphous state was also studied in the crystallization temperature range of 22–30 °C. The samples were first quenched to −40 °C to reach the amorphous state from the melt, and then heated to the crystallization temperature quickly as described in Section 2. The exothermal crystallization

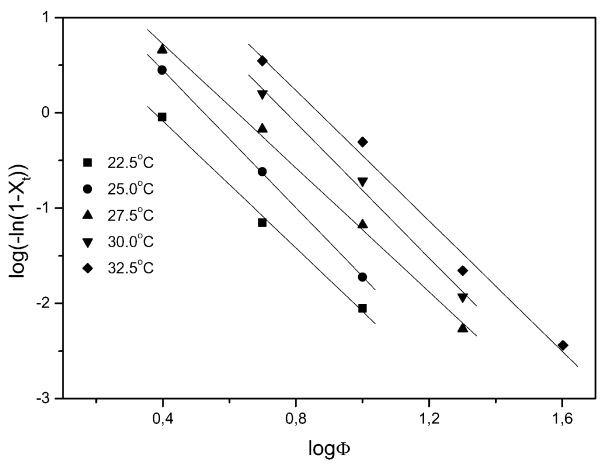

Fig. 7. Ozawa plots of PES during nonisothermal crystallization from the amorphous state.

Table 2
Nonisothermal crystallization kinetics of PES from the amorphous state based on the Ozawa equation

Crystallization temperature (°C)	n_o	$K(T)$ (°C/min)^n
22.5	3.33	1.76×10^1
25.0	3.61	7.78×10^1
27.5	3.25	1.06×10^2
30.0	3.54	5.34×10^2
32.5	3.42	9.37×10^2

n_o : Ozawa exponent, $K(T)$: the heating function.

curves of heat flow as a function of time were recorded and investigated. The plots of relative crystallinity X_t versus the crystallization time t were shown in Fig. 9. The crystallization process finished quickly in less than 8 min for all T_c. The Avrami equation, which was often used to analyze the isothermal crystallization kinetics for polymers [19,20], was employed to describe the crystallization behaviour of PES crystallized isothermally from the amorphous state. From the plots of $\log(-\ln(1 - X_t))$ versus $\log t$ shown in Fig. 10, the Avrami exponents n_a and k_a were obtained and listed in Table 3. It could be seen from Table 3 that the Avrami exponent n_a was between 2.0 and 3.0 for the isothermal crystallization of PES, which suggested that the crystallization might correspond to a spherical diffusion control growth with thermal nucleation [17]. From Table 3, it could also be seen that the crystallization rate constant k_a increased with the crystallization temperature. This was an expected behaviour, since in the diffusion controlled crystallization temperature range, the higher the crystallization temperature, the faster the crystallization rate.

The half-life crystallization time $t_{0.5}$, the time required to achieve 50% of the final crystallinity of the samples, is an important parameter for the discussion of crystallization kinetics. Usually, the crystallization rate is described as the reciprocal of $t_{0.5}$, namely $1/t_{0.5}$. The value of $t_{0.5}$ was

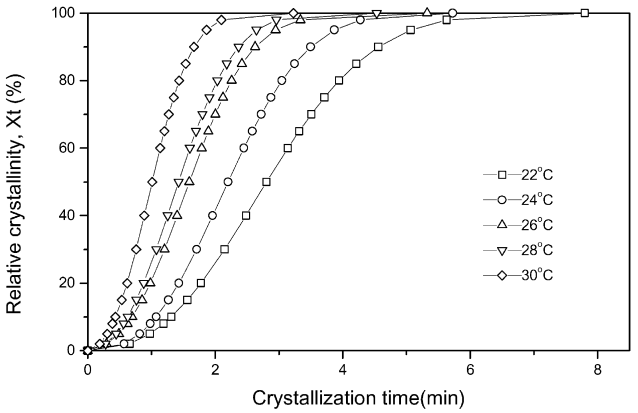

Fig. 9. Plots of relative crystallinity versus crystallization time for PES during isothermal crystallization from the amorphous state.

calculated by the following equation:

$$t_{0.5} = (\ln 2/k)^{1/n} \quad (8)$$

where k and n are the same as in the Avrami equation. Fig. 11 showed the temperature dependence of $t_{0.5}$ and $1/t_{0.5}$. It is clear that $t_{0.5}$ decreased with the crystallization temperature, while $1/t_{0.5}$ increased with the crystallization temperature for the isothermal crystallization of PES from the amorphous state. This indicated again that the isothermal crystallization rate of PES increased with the crystallization temperature in the diffusion controlled crystallization temperature range.

The samples were heated to 150 °C at a heating rate of 20 °C/min after they crystallized isothermally at 22–30 °C completely. Fig. 12 showed the melting behaviour of PES. Similar to the melting behaviour of nonisothermally crystallized PES samples, a small exothermal peak located at around 75 °C was observed just before the final endothermal melting for all the isothermally crystallized PES. The small exothermal peak increased gradually 74 to 76.5 °C when the crystallization temperature increased from

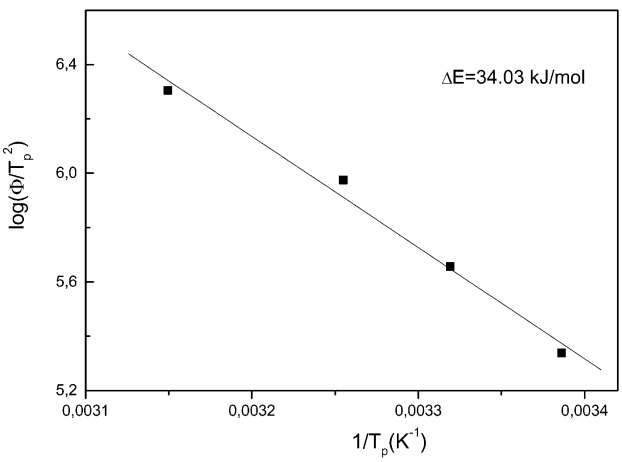

Fig. 8. Kissinger plot of PES for the estimation of ΔE in nonisothermal crystallization.

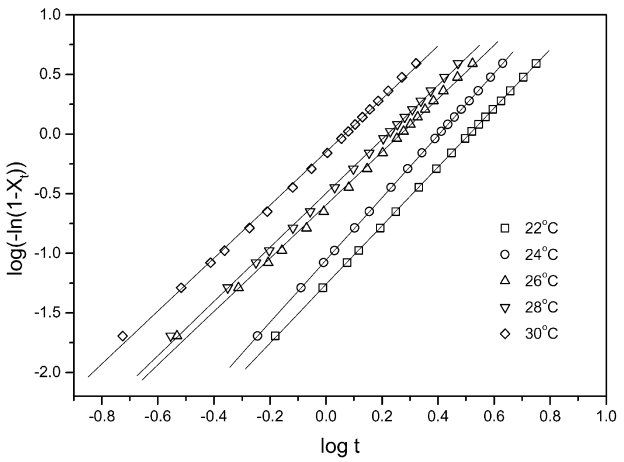

Fig. 10. Avrami plots of PES during isothermal crystallization from the amorphous state.

Table 3
Isothermal crystallization kinetics of PES from the amorphous state based on the Avrami equation

Crystallization temperature (°C)	Avrami exponent, n_a	Crystallization rate constant, k_a (min^{-n})
22	2.46	5.47×10^{-2}
24	2.61	8.77×10^{-2}
26	2.23	0.253
28	2.27	0.318
30	2.22	0.706

22 to 30 °C. The origin of this crystallization exotherm will be discussed in Section 3.3.

3.3. The origin of the crystallization exotherm just prior to the final melting of the crystals formed during nonisothermal and isothermal crystallization of PES from the amorphous state

In previous sections, we found that there was a minor crystallization exotherm appeared at high temperature just prior to the final melting of PES both in nonisothermal crystallization and in isothermal crystallization for PES from the amorphous state. In this section, we discuss the possible origin of this crystallization exotherm.

Two possibilities were considered to explain the origin of the crystallization exotherm. One possibility is that there are two kinds of polymer chains with different mobility in PES, namely, polymer chains with high molecular mobility and polymer chains with low molecular mobility. If the crystallization is performed at low crystallization temperature, the molecular mobility is reduced and the crystal growth rate is lower compared with the nucleation rate. As a result, an elevated number of small crystals will develop, resulting in a high amount of interconnected chains between the crystals that are not able to be absorbed in the lamellar thickness. Compared with the bulk of the amorphous phase, these tie chains have lower mobility. The presence of immobilized amorphous chain segments has been found in several semicrystalline polymers, i.e. poly(L-lactide) and polyethylene terephthalate [21,22]. In the case of PES, it was found there was a small exothermal peak just before the final melting and it might be explained by the possible presence of the amorphous chains with low molecular mobility. During the nonisothermal crystallization of PES from the amorphous state at low heating rate, only the amorphous chains with high molecular mobility were able to rearrange to crystallize at low temperature range, resulting in the real cold crystallization; whereas the amorphous chains with low molecular mobility were also able to crystallize at high temperature range since the molecular mobility of the amorphous chains increased with the temperature, resulting in the minor crystallization exotherm at high temperature range. During the isothermal crystallization of PES from the amorphous state at the low crystallization temperatures, i.e. 22–30 °C, only the amorphous chains with high molecular mobility were able to rearrange to crystallize, while the amorphous chains with low molecular mobility were still restricted and not able to disentangle and crystallize until they reached to a high temperature and gain the molecular mobility during the DSC heating scan after the completeness of the isothermal crystallization, which resulted in the appearance of the minor crystallization exotherm prior to the final melting of PES.

The other possibility is that the minor crystallization exotherm found both in the nonisothermal crystallization and in the isothermal crystallization originated from the melt-recrystallization of the unstable crystals formed earlier. The crystals formed through both the nonisothermal crystallization and isothermal crystallization has different thermal stability. Some crystals with low thermal stability

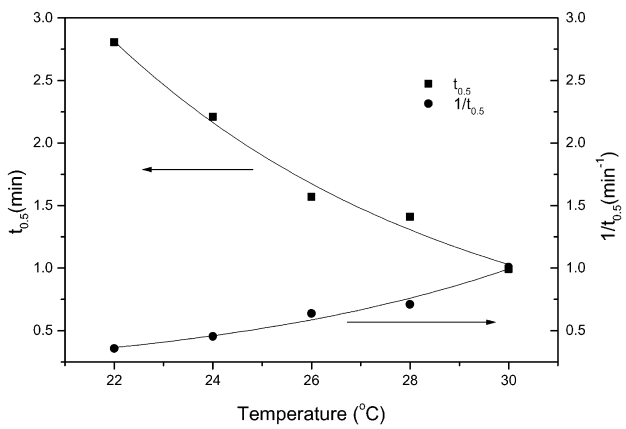

Fig. 11. Temperature dependence of $t_{0.5}$ and $1/t_{0.5}$ for PES isothermally crystallized from the amorphous state.

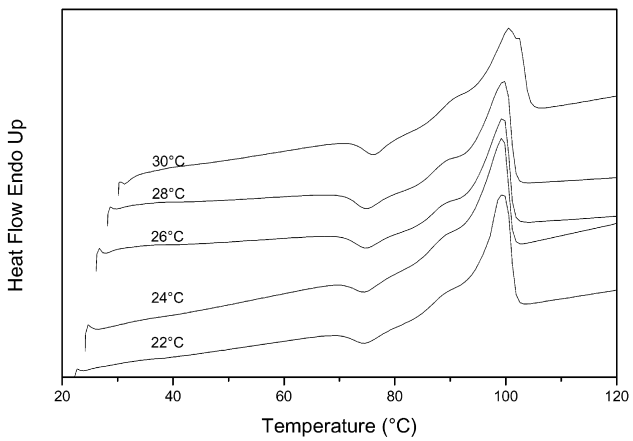

Fig. 12. Melting traces of the isothermally cold crystallized PES.

were able to recrystallize upon the DSC heating to the high temperature range. The others with high thermal stability corresponded to the final melting.

It seems that both the two possibilities could explain the experimental results found in this paper; however, it is really interesting to know that which one is the exact origin of the minor crystallization exotherm. So, we studied the non-isothermal and isothermal crystallization of PES again with temperature modulated differential scanning calorimetry (TMDSC) to understand better the origin of the crystallization exotherm.

TMDSC is a new thermal analysis technique, which applies a sinusoidal temperature oscillation (modulation) on a linear heating/cooling conventional DSC and makes the total heat flow (such as that from conventional DSC) to be separated into the heat capacity-related (reversible) and kinetic (nonreversible) components. Thus the endothermic signals can be detected in both reversible and nonreversible scans, whereas the crystallization exotherms only contribute to the nonreversible signal. This makes TMDSC a very powerful technique for the separation of exotherms (including crystallization and recrystallization) from glass transitions, reversible melting, or other heat capacity related events [23–27].

The nonisothermal and isothermal crystallization processes studied by TMDSC were the same as those by conventional DSC described in Section 2, except that the heating rate 2 °C/min was used with the oscillation amplitude of 0.5 °C and the oscillation period of 40 s throughout the investigation.

Fig. 13 showed the TMDSC curves of PES nonisothermally crystallized from the amorphous state at 2 °C/min. The total heat flow (bottom curve) can be separated into the well-defined nonreversible heat flow (top curve) and the reversible heat flow (middle curve). It could be seen in Fig. 13 that the major crystallization exothem located at low temperature range (peak at ca. 29 °C) and the minor crystallization exotherm located at high temperature range (peak at ca. 74 °C) appeared both in the total curve and in the nonreversible curve. But it should be noted that in the reversible curve there did appear a small endotherm with the peak at ca. 74 °C, corresponding to the position of the minor crystallization exotherm found in the total and nonreversible curves, prior to the final melting endothem. This indicated that the minor crystallization exotherm was the melt-recrystallization of the crystals with low thermal stability and not the crystallization of the amorphous chains with low molecular mobility.

Fig. 14 showed the TMDSC curves of PES isothermally crystallized from the amorphous state at 26 °C at 2 °C/min. Similar to the results found in Fig. 13, one small melting endotherm located at ca. 75 °C was found in the reversible curve, and the minor crystallization exotherm located at ca. 75 °C was found both in the total and nonreversible curves. This indicated again that the minor crystallization exotherm was the melt-recrystallization of the crystals with low thermal stability and not the crystallization of the amorphous chains with low molecular mobility.

In conclusion, there is no doubt TMDSC offers the direct evidence that the origin of the minor crystallization exotherm was from the melt-recrystallization of the originally existed unstable crystals formed through previous crystallization.

4. Conclusions

The nonisothermal crystallization kinetics of PES from the amorphous state were studied by DSC. Several methods, such as Avrami equation, Ozawa equation and Tobin equation, were applied to describe the nonisothermal crystallization process of PES. The isothermal cold crystallization of PES was also studied by the Avrami equation. It was found that there appeared two crystallization exotherms

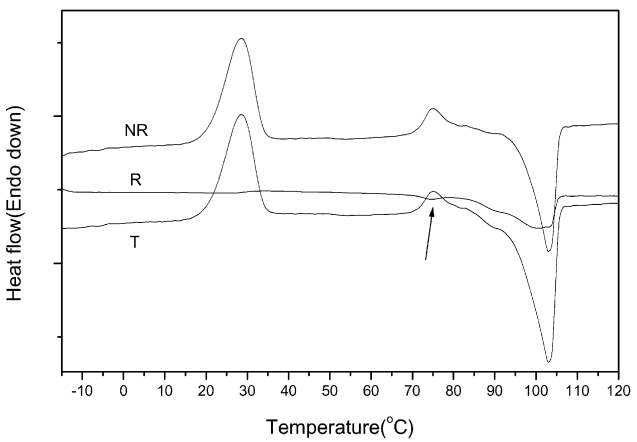

Fig. 13. TMDSC traces of PES nonisothermally crystallized from the amorphous state at 2 °C/min. The three curves from the top to the bottom are nonreversible heat flow (NR), reversible heat flow (R), and total heat flow (T), respectively.

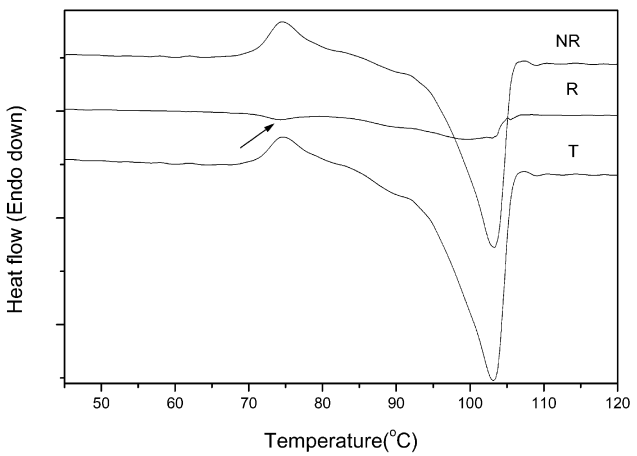

Fig. 14. TMDSC traces of PES at 2 °C/min after isothermally crystallized at 26 °C. The three curves from the top to the bottom are nonreversible heat flow (NR), reversible heat flow (R), and total heat flow (T), respectively.

when PES crystallized nonisothermally from the amorphous state. The major crystallization located at low temperature range corresponded to the real cold crystallization of PES, and the other minor one located at high temperature range was from the melt-recrystallization of the unstable crystals formed earlier. And the minor crystallization exotherm appeared too in the DSC trace upon heating to the melt after the isothermal crystallization finished completely and was also explained as the melt-recrystallization of the unstable crystals formed earlier. TMDSC experimental results offered the direct evidence that the origin of the minor crystallization exotherm was from the melt-recrystallization of the originally existed unstable crystals formed through previous crystallization.

Acknowledgements

Part of this work was supported by Grant-in-Aid for Scientific Research on Priority Areas (A) 'Dynamic Control of Strongly Correlated Soft Materials' (No. 413/13031012) from the Ministry of Education, Science, Sports, Culture, and Technology, Japan. Z. Qiu thanks the Japan Society for the Promotion of Science for providing the fellowship and grant-in-aid to do this research at The University of Tokyo and Tokyo Institute of Technology.

References

[1] Ha CS, Cho WJ. Prog Polym Sci 2002;27:759.
[2] Fuller CS, Erickson CL. J Am Chem Soc 1937;59:344.
[3] Ueda AS, Chatani Y, Tadokoro H. Polym J 1971;2:387.
[4] Iwata T, Doi Y, Isono K, Yoshida Y. Macromolecules 2001;34:7343.
[5] Ichikawa Y, Washiyama J, Moteki Y, Noguchi K, Okuyama K. Polym J 1995;27:1264.
[6] Al-Raheil IA, Qudah AMA. Polym Int 1995;37:249.
[7] Gan Z, Abe H, Doi Y. Biomacromolecules 2000;1:704.
[8] Al-Salah HA. Polym Bull 1998;41:593.
[9] Chen HL, Wang SF. Polymer 2000;41:5157.
[10] Qiu ZB, Ikehara T, Nishi T. Macromolecules 2002;35:8541.
[11] Avrami M. J Chem Phys 1939;7:1103.
[12] Tobin MC. J Polym Sci, Polym Phys 1974;12:399.
[13] Ozawa T. Polymer 1971;12:150.
[14] Cebe P. Polym Compos 1988;9:271.
[15] de Juana R, Jauregui A, Calahorra E, Cortázar M. Polymer 1996;37:3339.
[16] Supaphol P. J Appl Polym Sci 2000;78:338.
[17] Wunderlich B, Macromolecular physics, vol. 2. New York: Academic Press; 1976.
[18] Kissinger HE. J Res Nat Bur Stand 1956;57:217.
[19] Qiu ZB, Mo ZS, Zhang HF, Sheng SR, Song CS. J Macromol Sci—Phys 2000;B39:373.
[20] Qiu ZB, Mo ZS, Zhang HF, Sheng SR, Song CS. J Polym Sci, Polym Phys 2000;38:1992.
[21] Iannace S, Nicolais L. J Appl Polym Sci 1997;64:911.
[22] Coburn JC, Boyd RH. Macromolecules 1986;19:2238.
[23] Toda A, Tomita C, Hikosaka M, Saruyama Y. Polymer 1998;39:5093.
[24] Okazaki I, Wunderlich B. J Polym Sci, Polym Phys 1996;34:2941.
[25] Okazaki I, Wunderlich B. Macromol Rapid Commun 1997;18:313.
[26] Yuan ZH, Song R, Shen DY. Polym Int 2000;49:1377.
[27] Qiu ZB, Ikehara T, Nishi T. Polymer 2003;44:3095.